Optimisation of a modified acoustic black hole profile for the reduction of dynamic stress

A. Keys, J. Cheer
ISVR, University of Southampton University Road, Highfield
Southampton, UK, SO17 1BJ
e-mail: **a.keys@soton.ac.uk**

Abstract

Acoustic Black Holes (ABHs) make use of structural modifications to effectively reduce the wave speed of vibration in a structure. This increases the effectiveness of damping material applied to the ABH and results in more effective vibration control. The most common realisation of an ABH is to gradually taper the thickness of a structure, resulting in a very thin tip when realised as a structural termination. The ABH effect causes an increase in energy density as structural thickness decreases, resulting in a large amount of energy being focused within the thin section of the ABH. This raises concerns around high levels of dynamic stress in the structure. This paper presents a modified ABH taper profile that aims to reduce the level of dynamic stress in the structure while maintaining ABH performance. This is achieved by increasing the thickness of the taper at points of high stress. The parameters defining the modified ABH profile are optimised to reduce dynamic stress in the taper while maintaining ABH performance, and the optimised profile is compared to the conventional ABH for both performance measures.

1 Introduction

The attenuation of structural vibration is often desirable in engineering applications and is commonly achieved using one of two traditional techniques. The mass of the structure can be increased in order to reduce vibration, but this conflicts with modern engineering approaches that aim for lightweight structures. Another commonly used technique is to add damping to the structure to dissipate the energy from structural vibration, however, this method is only effective when the wavelength of vibration is comparable to the size of the applied damping treatment. Acoustic Black Holes (ABHs) are able to attenuate structural vibration while overcoming both of these limitations, by introducing modifications to the structure such that the frequency range over which an applied damping treatment is effective is increased, without an increase in mass.

The initial concept for the ABH was proposed by Mironov [1], who defined an ABH as a tapered edge of a plate, starting at the thickness of the plate and ending with zero thickness at the edge. Since the speed of a wave travelling through a plate or a beam is proportional to the square root of its thickness, when a power law of two is used to define the decrease in thickness a linear decrease in wavespeed occurs, reducing to zero at the tip. This theoretical case, therefore, results in a zero reflection condition at the edge of the plate, but in practice it is not possible to manufacture a structure that tapers to a zero thickness, and so a finite tip height must be considered. This was first implemented experimentally by Krylov [2] who demonstrated that applying a viscoelastic damping layer to the ABH taper provides significant vibration attenuation despite a finite tip height. This is because the incident structural wave is slowed down in the ABH taper and the wavelength at a fixed frequency is reduced, resulting in an increase in the frequency range over which the applied damping treatment is effective.

The ability of ABHs to attenuate vibration in structures has been widely demonstrated in the literature both numerically [3, 4, 5] and experimentally [6, 7, 8], however, the ABH effect inherently results in high amplitude vibration in the thinnest part of the structure. Although this characteristic has been utilised advantageously in the field of energy harvesting [9, 10], the resulting high levels of dynamic stress raise concerns

about structural fatigue in the ABH taper, especially in applications with a high amplitude excitation. The level of fatigue in an ABH structure has previously been assessed in a numerical study [11] and the level of dynamic stress in an ABH taper has been measured experimentally [12]. A modified ABH taper profile for the reduction of fatigue has also been proposed using a numerical model to optimise the profile for the reduction of fatigue while maintaining ABH performance [13].

This paper builds on the work presented in [13] by implementing a modified ABH profile with parameters that have been optimised to reduce the level of dynamic stress in the taper while maintaining ABH vibration control performance. Section 2 describes the numerical model used to assess the performance of the ABH in terms of both vibration attenuation and dynamic stress. Section 3 introduces the modified ABH profile and how it is defined parametrically, before explaining the optimisation procedure used to minimise dynamic stress while maintaining ABH performance. Section 4 presents the results of the numerical study, comparing both the conventional and modified ABHs in terms of reflection coefficient and dynamic stress. Section 5 draws conclusions from the results.

2 Numerical model

This work studies an ABH used to terminate an aluminium beam with a uniform, rectangular cross-section. The geometry of the structure is shown in Figure 1 and the parameters used to define it are listed in Table 1. A 2D finite element model of the structure has been implemented using COMSOL multiphysics software, where the structure is defined in the x and y planes, with a prescribed thickness in the $z-$ plane. The uniform beam section of the structure has a thickness of h_0, and the thickness of the ABH section, $h(x)$, is defined by

$$h(x) = \left(\frac{l_{ABH} - x}{l_{ABH}}\right)^{\mu} \left(h_0 - h_{tip}\right) + h_{tip}. \tag{1}$$

Free boundary conditions have been applied at the edges of the structure and a distributed force, F, is applied in the $z-$axis direction, evenly distributed over a ring with an inner radius of 6 mm and an outer radius of 12 mm. The center of the ring is located 0.02 m from the non-ABH end of the beam. This specific forcing has been modelled to represent the experimental configuration that is the subject of future work.

2.1 Damping

It has been shown that both the quantity of damping and the region over which it is applied have a significant impact on ABH performance [6]. It is therefore necessary, if the results obtained from this simulation-based study are to provide practical insight, that the damping applied in the numerical model approximates the behaviour of a viscoelastic damping layer that might be applied to an experimentally realised structure. The numerical model implements damping in the ABH taper region as an isotropic loss factor, $\eta(x, y)$, applied to the taper rather than as an explicitly modelled damping layer. Therefore, the isotropic loss factor is scaled so that a higher value of η is implemented closer to the ABH tip, where the structure is thinner in order to represent a damping layer of constant thickness. The loss factor is thus scaled according to

$$\eta(x, y) = \frac{h_{tip}}{h(x, y)}, \tag{2}$$

noting that the damping can change with both x and y since the modified profile has a thickness profile that varies across the width of the structure. It is also important that the overall amount of damping in the structure stays consistent between the conventional and modified ABH profiles, so the loss factor is also scaled according to the ratio of the volumes of the conventional and modified profiles. The stiffness of the ABH taper is also changed according to the thickness of the profile in order to account for the increase in stiffness due to an evenly applied damping layer, which becomes significant in regions where the structure is

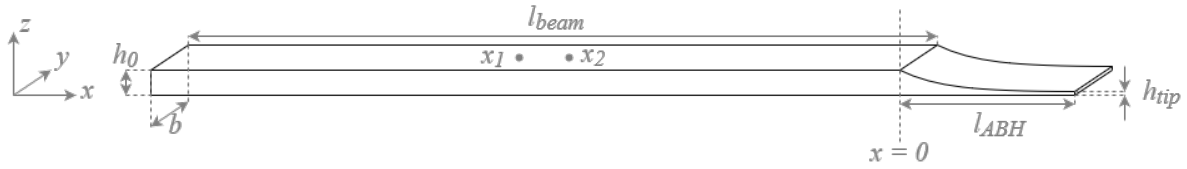

Figure 1: Beam with ABH termination: definition of geometric parameters.

Table 1: Values of the parameters defining the geometry shown in Figure 1 and the model.

Parameter	Symbol	Value
Beam thickness	h_0	10 mm
Beam length	l_{beam}	300 mm
Beam width	b	40 mm
ABH taper length	l_{ABH}	70 mm
ABH power law	μ	4
ABH tip height	h_{tip}	0.6 mm
Excitation force	F	1 N

very thin. This is achieved by increasing the Young's modulus in the ABH profile to an equivalent stiffness, E_{eq}, that accounts for the damping layer, according to

$$E_{eq} = E_a + \frac{t_d}{h(x,y)^3}\left[E_d t_d^2 + 12E_d\left(\frac{h(x,y)+t_d}{2}\right)^2\right], \tag{3}$$

where E_a is the Young's modulus of aluminium, E_d is the Young's modulus of 'Yellow plastic compound' and $t_d = 2$ mm is the thickness of the damping layer being approximated. An evenly distributed mass of 11.9 g has been applied to the ABH taper to account for the additional mass of an experimentally applied damping layer. The assumed properties of the viscoelastic damping layer that result in the modification to the stiffness, mass and damping of the ABH taper section of the structure are based on 'Yellow plastic compound' manufactured by WT Henley [14], which has previously been applied to experimentally realised ABH structures [7, 12].

2.2 Performance metrics

This section outlines the performance metrics that are used to evaluate the performance of the modified and conventional ABH profiles in terms of vibration control and dynamic stress. These metrics also form the basis of the cost function utilised to optimise the modified ABH profiles.

2.2.1 Reflection coefficient

A useful way to quantify vibration attenuation for an ABH applied to the end of a beam is to use the reflection coefficient, R, which is the ratio of the incident and reflected travelling waves in the $x-$direction of the structure. This is calculated here using the method outlined in [15], where the transverse velocity of the beam at two points along its length, x_1 and x_2, as shown in Figure 1, are used to calculate the complex amplitudes of the positive and negative propagating waves in the structure as

$$\Phi^+ = \frac{-1}{2\omega \sin\left(k_f \Delta_x\right)}\left[\dot{w}(x_1)e^{ik_f\Delta_x/2} - \dot{w}(x_2)e^{-ik_f\Delta_x/2}\right], \tag{4}$$

$$\Phi^- = \frac{-1}{2\omega \sin(k_f \Delta_x)} \Big[\dot{w}(x_2) e^{ik_f \Delta_x/2} - \dot{w}(x_1) e^{-ik_f \Delta_x/2} \Big], \tag{5}$$

where $\dot{w}(x)$ is the velocity of the beam in the z-direction at point x, Φ^+ and Φ^- are the complex amplitudes of the positive and negative going waves respectively, k_f is the flexural wavenumber in the beam section, ω is the angular frequency, Δ_x is the separation between the two points x_1 and x_2 and i is the unit imaginary number. The complex amplitudes of the positive and negative going waves can then be used to calculate the reflection coefficient as

$$|R| = \left| \frac{\Phi^-}{\Phi_+} \right|. \tag{6}$$

In this work, the reflection coefficient is evaluated over a frequency range of 100 Hz to 10 kHz. In the optimisation process described in Section 3, the broadband averaged reflection coefficient, $\overline{R}$, over this frequency range is used to compare the vibration control performance of the optimised modified ABH profiles to the conventional ABH profile.

2.2.2 Stress

The motivation behind reducing the dynamic stress considered here is that, in practical applications with high amplitude excitation, the structural fatigue of an ABH could become significant. The point on a structure most likely to experience failure due to fatigue is the point at which the level of dynamic stress is highest across both position, $\mathbf{x} = [x, y]$, and frequency, f. The maximum dynamic stress experienced by the ABH taper, σ_{max}, is defined as

$$\sigma_{max} = \max_{\mathbf{x}, f} \big[\sigma(\mathbf{x}, f) \big], \tag{7}$$

where $\sigma(\mathbf{x}, f)$ is the stress in the ABH taper as a function of position and frequency. The position at which σ_{max} occurs is $\mathbf{x}_{max}$, meaning that the dynamic stress response can then be evaluated across frequency at position $\mathbf{x}_{max}$ to give

$$\sigma_{x,max}(f) = \sigma(\mathbf{x}_{max}, f). \tag{8}$$

The stress presented in the subsequent section has been evaluated over a frequency range of 100 Hz to 10 kHz, however the stress above 3 kHz is not considered in the optimisation process since the level of dynamic stress at higher frequencies is significantly lower than in the frequency range considered. The optimisation process described in Section 3 uses the RMS value of $\sigma_{x,max}(f)$, denoted σ_{RMS}, to quantify the stress reduction achieved by the optimised ABH profile over frequency.

3 Modified ABH profile

The modified ABH profile implemented in this work is based on the profile proposed in [13], where the thickness of the modified profile is increased along the edges such that it is thicker where the fatigue was found to be higher in a conventional ABH profile. The modified profile, $h_{mod}(x, y)$, is defined by multiplying the conventional ABH thickness profile, $h(x)$, by a parametrically defined multiplier, $M(x, y)$. The multiplier is defined in terms of trigonometric functions as

$$M(x, y) = -A \cos\left(\frac{\pi x^n}{l_{ABH}^n} - \frac{\pi}{2} \right) \cos\left(\frac{\pi y}{b} - \frac{\pi}{2} \right) + Am \cos\left(\frac{\pi x^n}{l_{ABH}^n} - \frac{\pi}{2} \right) + 1, \tag{9}$$

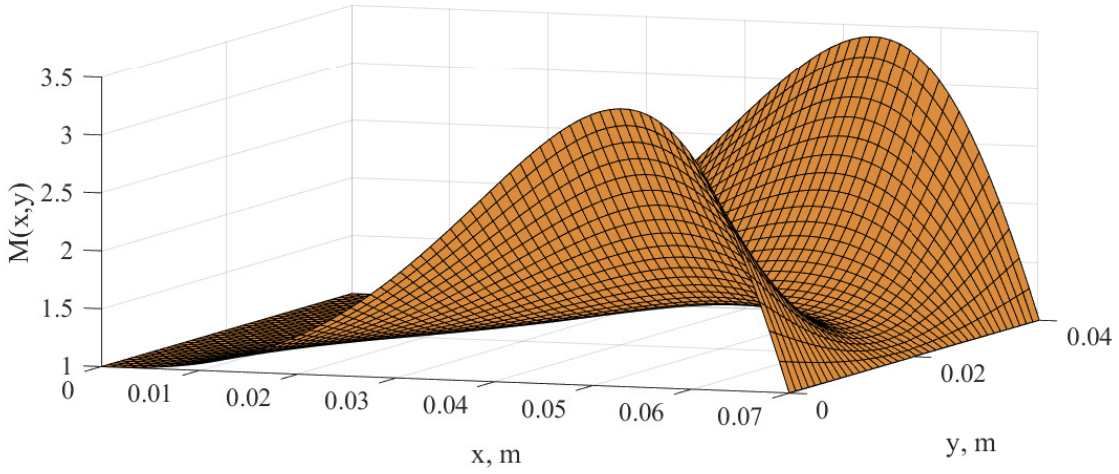

Figure 2: $M(x, y)$ with parameter values of $A = 2$, $n = 2.5$ and $m = 1.2$ plotted across the range of x and y over which the taper is defined.

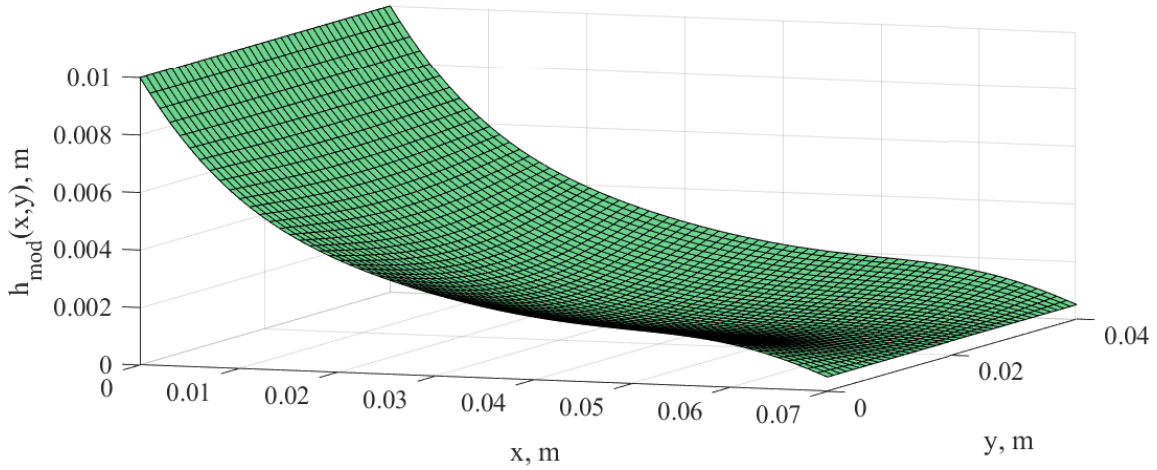

Figure 3: $h_{mod}(x, y)$ plotted for parameter values of $A = 2$, $n = 2.5$ and $m = 1.2$ across the range of x and y over which the taper is defined.

where A, n and m are scalar parameters. A defines the amplitude of the modification to the profile, n defines the position at which the peaks in the raised section of the profile occur and m defines the thickness of the profile along the centre line of the taper. The multiplier, $M(x, y)$, is shown in Figure 2 and the modified profile, $h_{mod}(x, y)$, is shown in Figure 3, both with parameter values of $A = 2.0$, $n = 2.5$ and $m = 1.2$.

3.1 Optimisation

The aim of the optimisation process is to determine the parameters that define the modified profile, A, n and m, that reduce the level of dynamic stress in the ABH taper, while largely maintaining the reflection coefficient performance of the conventional profile. The cost function, J, used in this work is defined as

$$J = \frac{\left[\int_{f_{min}}^{f_{max}} \sigma^k_{x,max,mod}(f)\, df\right]^{0.5}}{\left[\int_{f_{min}}^{f_{max}} \sigma^k_{x,max,con}(f)\, df\right]^{0.5}}, \tag{10}$$

where $f_{min} = 100$ Hz and $f_{max} = 3$ kHz are the lower and upper frequency limits of the stress evaluation respectively, $\sigma_{x,max,con}(f)$ and $\sigma_{x,max,mod}(f)$ are the levels of dynamic stress at the point of maximum stress on the taper, as given by Equation (8), for the conventional and modified profiles respectively and k is a scalar allowing the stress to be raised to a higher power before the integral is taken. The square root of the integral is taken so that using a power of $k = 2$ results in the cost function being equal to the ratio of the RMS stress for the modified and conventional profiles.

To largely maintain the vibration control performance of the ABH, while minimising the cost function defined by Equation (8), the optimisation also includes a constraint on the reflection coefficient. In this optimisation, the ratio of the broadband averaged reflection coefficient for the modified profile, $\overline{R}_{mod}$, and the conventional profile, $\overline{R}_{con}$, is constrained by

$$\frac{\overline{R}_{mod}}{\overline{R}_{con}} < 1.1, \tag{11}$$

thus allowing an increase of up to 10% in the broadband averaged reflection coefficient.

3.1.1 Optimisation algorithms

There is a vast body of literature on the solution of constrained optimisation problems, such as that defined here. Gradient descent optimisation methods are known to be effective at finding a local minimum for non-linear problems [16], however, multiple randomly generated start points should be used to increase the likelihood of finding the global minimum in complex problem spaces [17]. The main drawback of this approach is that it is computationally expensive if the design space is large. One approach to overcoming this problem is provided by simulated annealing. Simulated annealing algorithms also make use of an iterative approach, however, in this case a temperature variable, T, is used to control the optimisation process [17]. Each iteration of the algorithm is found by 'jumping' from the current point in the design space to a nearby point, where the size of the jump is proportional to T. The algorithm then decides whether to accept this new point based on the value of the cost function, where if the new point shows an improvement then it is accepted. If, however, the cost function at the new point is higher than the cost function at the previous point, the algorithm will randomly decide whether to accept the new point, the probability of which is dictated by both the size of the increase in the cost function and the value of the temperature variable. The temperature variable decays exponentially as the optimisation goes on, allowing large jumps at the start of the optimisation to search a large portion of the design space, while allowing the algorithm to converge on a solution as the temperature decreases. It is also common to start a simulated annealing algorithm multiple times, known as reannealing, using random start points to ensure that a large portion of the design space is explored.

In this work, a hybrid optimisation is implemented, where a simulated annealing algorithm is first utilised to search a large portion of the design space to locate the region of a possible global minimum. The best result from the simulated annealing stage is then used as a start point for a gradient descent algorithm to more accurately determine the position of the minimum.

4 Results

The optimisation process described in the previous section has been utilised in conjunction with the numerical model described in Section 2 to determine the optimal parameters for the modified ABH profile. This section compares the performance of the conventional and modified ABH profiles in terms of reflection coefficient and dynamic stress.

The optimisation regime has been implemented for values of k of 1, 2 and 4, the results of which are shown in Table 2 in terms of the performance metrics σ_{RMS}, σ_{max} and $\overline{R}$ shown in terms of percentage change compared to the conventional ABH profile. It can be seen from these results that using a lower value of k results in a greater decrease in σ_{RMS} but also a greater increase in both σ_{max} and $\overline{R}$. This implies that a

Table 2: Results from the optimisations using values of $k = 1$, 2 and 4, listing the optimised parameters alongside the performance metrics in terms of percentage change compared to the conventional ABH profile.

Parameter	$k = 1$	$k = 2$	$k = 4$
A	1.14	1.54	0.59
n	1.61	1.65	3.79
m	1.30	1.12	1.65
σ_{RMS}	-38.1%	-34.3%	-20.4%
σ_{max}	$+23.7\%$	$+24.6\%$	$+5.1\%$
$\overline{R}$	$+9.5\%$	$+8.3\%$	$+7.5\%$

lower value of k is effectively able to reduce the RMS stress in the ABH taper, but only at the expense of an increase in both the maximum stress and the reflection coefficient. The use of a higher value of k in the optimisation process prioritises the reduction of the higher amplitude dynamic stress in the structure, which accounts for the less significant increase in σ_{max} observed when a cost function with $k = 4$ is used. For practical applications where fatigue is a concern, a higher value of k would be more suitable, since it is the higher amplitude dynamic stress that contributes most significantly to fatigue damage in a structure.

4.1 Reflection coefficient

To provide further insight into the behaviour of the conventional and modified ABH terminations, the reflection coefficient, R, has been calculated over frequency for each profile configuration using the method outlined in Section 2.2. The reflection coefficient is plotted from 100 Hz to 10 kHz for all of the profiles in Figure 4. It can be seen that all four profiles exhibit regular dips in the reflection coefficient which correspond to ABH taper modes, where the energy from a wave propagating along the beam is more effectively transferred into the ABH taper, resulting in more energy being dissipated by the structural damping. Another feature of the reflection coefficient that can be seen for all four profiles is the trend for a reduction with increasing frequency. At higher frequencies, the wavelength of vibration in the structure is shorter, and therefore more comparable to the size of the area over which the damping treatment is applied, resulting in more effective dissipation of energy. It can be seen that the frequency at which the dips in the reflection coefficient occur are more similar to the conventional profile for the $k = 4$ case, while for the $k = 1$ and $k = 2$ configurations result in a more significant shift. It can also be observed that the dips in the reflection coefficient are sharper for a value of $k = 4$, while for the $k = 1$ and $k = 2$ cases wider dips are observed that are more similar to the conventional profile. Despite these small differences in behaviour, the presence of regular dips and a trend to decrease with frequency in the reflection coefficient indicate that the general vibration control performance of the conventional ABH taper is conserved over frequency for all of the optimised modified profiles.

4.2 Stress

To provide further insight into the stress characteristics of the conventional and modified ABHs, the dynamic stress, $\sigma_{x,max}$, is plotted against frequency for all configurations in Figure 5. As with the reflection coefficient results, the dynamic stress for the $k = 1$ and $k = 2$ modified configurations are very similar, whilst the $k = 4$ configuration exhibits noticeably different behaviour. It can be seen that all three modified profiles effectively reduce the amplitude of the peaks in stress around 600 Hz and 1300 Hz, however, they all also result in an increase in the amplitude of the peak at around 450 Hz. The stress responses at this peak demonstrate the cause of the increase in σ_{max} shown in Table 2, where the $k = 1$ and $k = 2$ configurations exhibit a larger increase in the maximum stress amplitude compared to the $k = 4$ case. The most significant difference in the responses of the modified profiles is the frequency at which the second peak in the response occurs, which is significantly higher for the $k = 1$ and $k = 2$ cases compared to the $k = 4$ and conventional profiles. This shift in the frequency of the second peak away from the first peak appears to also result in the first peak becoming noticeably sharper, which is also likely to contribute to the higher values of σ_{max} observed for

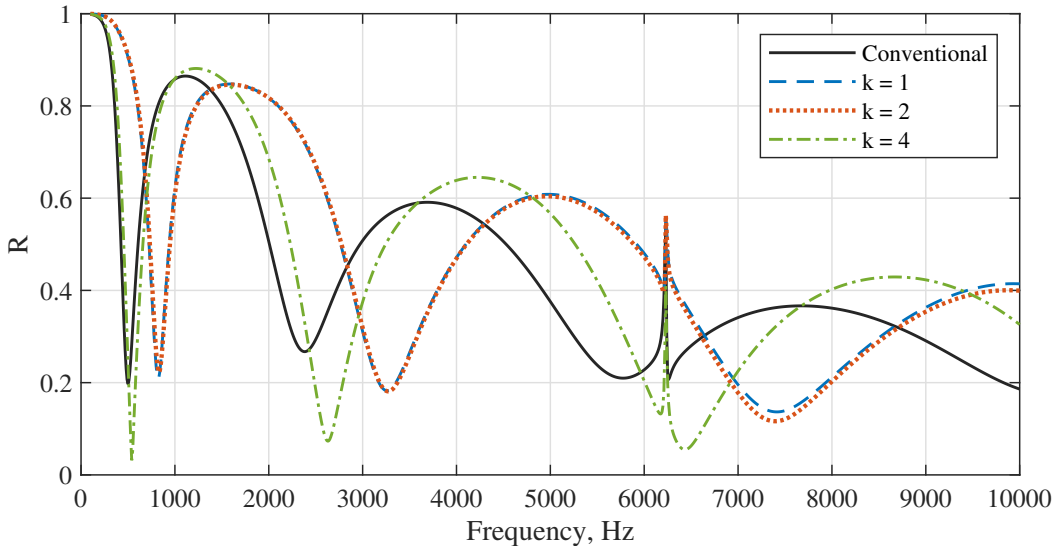

Figure 4: Reflection coefficient against frequency for the conventional ABH profile and the modified ABH profiles optimised using values of $k = 1$, 2 and 4 in the cost function.

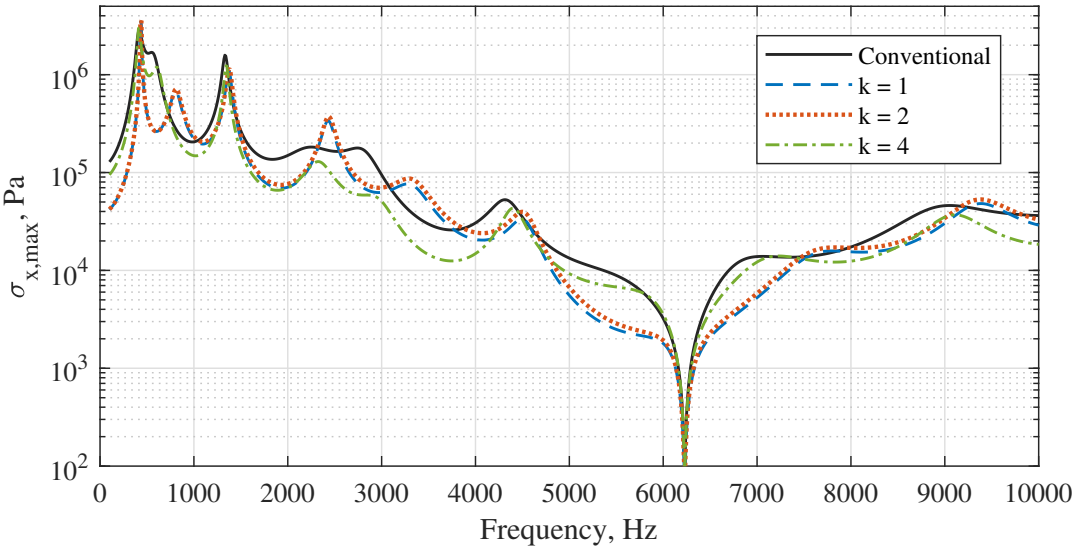

Figure 5: $\sigma_{x,max}$plotted against frequency for the conventional ABH profile and the modified ABH profiles optimised using values of $k = 1$, 2 and 4 in the cost function..

these cases. Since the optimisation has only considered the stress up to a frequency of 3 kHz, a low value of the cost function does not indicate low stress over the full frequency range shown in Figure 5. It can be seen, however, that all three of the modified profiles result in a reduction in the stress across the majority of the frequency range from 3 to 10 kHz.

Based on the reflection coefficient and dynamic stress results presented in this section, it can be concluded that the modified profiles are successful in reducing the RMS dynamic stress in the structure without significantly impacting the vibration control performance of the ABH. However, the results indicate that there is a trade-off between a decrease in the RMS dynamic stress and an increase in the maximum dynamic stress.

5 Conclusions

This paper has presented a modified ABH profile that has been optimised to reduce the dynamic stress in the ABH taper without significantly impacting the vibration control performance. A two stage optimisation process, implementing a simulated annealing algorithm followed by a gradient descent algorithm, has been used to reduce a cost function based on the dynamic stress in the ABH taper with a constraint on the reflection coefficient.

Three different versions of the cost function have been utilised in the optimisation process, with each raising the stress response to a power of 1, 2 or 4 before integration to vary the degree to which high amplitude dynamic stress in the structure is prioritised. The results show that there is a trade-off to be had between reducing the RMS stress in the structure and increasing both the maximum stress and the reflection coefficient. Low powers in the cost function result in a large reduction in the RMS stress, but also a significant increase in both the maximum stress and the reflection coefficient, while high powers in the cost function result in less reduction in the RMS stress, but effectively minimise the undesirable increase in the maximum stress and the reflection coefficient. It is unlikely that the modified profiles presented in this investigation would be suitable for practical applications where fatigue may be a concern due to the increase in the maximum stress. Since high amplitude stress contributes most significantly to structural fatigue, the increase in fatigue due to the maximum stress may outweigh the reduction in fatigue due to the decrease in the RMS stress. Further investigation into the use of different cost functions could determine if a reduction in both the RMS and maximum stress is feasible, however, this lies outside the scope of this paper.

Through examination of the reflection coefficient for the conventional and modified profiles, it has been shown that all of the profiles exhibit the basic characteristics of an ABH, with regular dips in the reflection coefficient corresponding to ABH taper modes and a trend for the reflection coefficient to decrease as frequency increases. This demonstrates that the ABH effect is conserved for the modified profiles.

It has been shown that all three modified profiles effectively reduce the amplitude of the second and third peaks in the stress response of the structure, however, they also increase the amplitude of the first peak compared to the conventional ABH profile. Powers of 1 and 2 used in the cost function result in the second peak being significantly shifted in frequency, which appears to cause the first peak to become sharper and contribute towards the higher maximum stress in the structure. The use of a power of 4 in the cost function results in a much smaller shift in the frequency of the second peak and a smaller increase in the maximum stress.

Acknowledgements

This work was partially supported by the Intelligent Structures for Low Noise Environments (ISLNE) EPSRC Prosperity Partnership (EP/S03661X/1) and partially by the Department of Science, Innovation and Technology (DSIT) Royal Academy of Engineering under the Research Chairs and Senior Research Fellowships programme.

References

[1] M. A. Mironov, "Propagation of a flexural wave in a plate whose thickness decreases smoothly to zero in a finite interval," *(in English) Soviet Physics Acoustics - USSR*, vol. 34(3), pp. 318–319, 1988.

[2] V. V. Krylov and F. J. B. S. Tilman, "Acoustic 'black holes' for flexural waves as effective vibration dampers," *Journal of Sound and Vibration*, vol. 274(3), pp. 605–619, 2004.

[3] P. Feurtado and S. Conlon, "Investigation of boundary-taper reflection for acoustic black hole design," *Noise Control Engineering Journal*, vol. 63(5), pp. 460–466, 2015.

[4] J. Y. Lee and W. Jeon, "Vibration damping using a spiral acoustic black hole," *Journal of the Acoustical Society of America*, vol. 141, 2017.

[5] V. V. Krylov, "Propagation of plate bending waves in the vicinity of one- and two-dimensional acoustic 'black holes'," *Proceedings of the ECCOMAS Thematic Conference on Computation Methods in Structural Dynamics and Earthquake Engineering*, 2007.

[6] V. V. Krylov and R. E. Winward, "Experimental investigation of the acoustic black hole effect for flexural waves in tapered plates," *Journal of Sound and Vibration*, vol. 300, 2007.

[7] K. Hook, J. Cheer, and S. Daley, "A parametric study of an acoustic black hole on a beam," *Journal of the Acoustical Society of America*, vol. 145(6), pp. 3488–3498, 2019.

[8] V. B. Georgiev, J. Cuenca, F. Gautier, L. Simon, and V. V. Krylov, "Damping of structural vibrations in beams and elliptical plates using the acoustic black hole effect," *Journal of Sound and Vibration*, vol. 330, 2011.

[9] L. Zhao, S. C. Conlon, and F. Semperlotti, "An experimental study of vibration based energy harvesting in dynamically tailored structures with embedded acoustic black holes," *Smart Materials and Structures*, vol. 24, 2015.

[10] H. Ji, X. Wang, J. Qiu, L. Cheng, Y. Wu, and C. Zhang, "Noise reduction inside a cavity coupled to a flexible plate with embedded 2-d acoustic black holes," *Journal of Sound and Vibration*, vol. 455, 2019.

[11] A. Keys and J. Cheer, "Fatigue analysis of an acoustic black hole," *Proceedings of the 28th International Congress on Sound and Vibration*, JUL 2022.

[12] A. Keys and J. Cheer, "Experimental measurements of stress in an acoustic black hole using a laser doppler vibrometer." *Proceedings of Meetings on Acoustics*, DEC 2023.

[13] A. Keys and J. Cheer, "Modified acoustic black hole profile for improved fatigue performance," *Proceedings of the 51st International Congress and Exposition on Noise Control Engineering*, AUG 2022.

[14] W. T. Henley, https://www.wt-henley.com/cable_accessories-green_and_yellow_plastic_compound.html, accessed: 2024-04-05.

[15] V. Denis, F. Gautier, A. Pelat, and J. Poittevin, "Measurement and modelling of the reflection coefficient of an abh termination," *Journal of Sound and vibration*, vol. 349, 2015.

[16] H. B. Curry, "The method of steepest descent for non-linear minimization problems," *Quarterly Applied Mathematics*, vol. 2, 1944.

[17] S. Kirkpatrick, C. D. Gelatt, and M. P. Vecchi, "Optimisation by simulated annealing," *Science*, vol. 220, 1983.